A biophysical study of the interactions between the antimicrobial peptide indolicidin and lipid model systems

Nielsen, Josefine Eilsø; Lind, Tania Kjellerup; Lone, Abdullah; Gerelli, Yuri; Hansen, Paul Robert; Jenssen, Håvard; Cárdenas, Marité; Lund, Reidar

Published in:
B B A - Biomembranes

DOI:
10.1016/j.bbamem.2019.04.003

Publication date:
2019

Document Version
Publisher's PDF, also known as Version of record

Citation for published version (APA):
Nielsen, J. E., Lind, T. K., Lone, A., Gerelli, Y., Hansen, P. R., Jenssen, H., Cárdenas, M., & Lund, R. (2019). A biophysical study of the interactions between the antimicrobial peptide indolicidin and lipid model systems. *B B A - Biomembranes*, *1861*(7), 1355-1364. https://doi.org/10.1016/j.bbamem.2019.04.003

BBA - Biomembranes 1861 (2019) 1355–1364

Contents lists available at ScienceDirect

BBA - Biomembranes

journal homepage: www.elsevier.com/locate/bbamem

A biophysical study of the interactions between the antimicrobial peptide indolicidin and lipid model systems

Josefine Eilsø Nielsen[a], Tania Kjellerup Lind[b], Abdullah Lone[c], Yuri Gerelli[d], Paul Robert Hansen[e], Håvard Jenssen[c], Marité Cárdenas[b], Reidar Lund[a,*]

[a] Department of Chemistry, University of Oslo, 0315 Oslo, Norway
[b] Biofilms Research Center for Biointerfaces, Department of Biomedical Science, Health and Society, Malmö University, 20506 Malmö, Sweden
[c] Department of Science and Environment, Roskilde University, 4000 Roskilde, Denmark
[d] Institut Laue - Langevin, 38000 Grenoble, France
[e] Department of Drug Design and Pharmacology, University of Copenhagen, 2100 Copenhagen, Denmark

A B S T R A C T

The naturally occurring peptide indolicidin from bovine neutrophils exhibits strong biological activity against a broad spectrum of microorganisms. This is believed to arise from selective interactions with the negatively charged cytoplasmic lipid membrane found in bacteria. We have investigated the peptide interaction with supported lipid model membranes using a combination of complementary surface sensitive techniques: neutron reflectometry (NR), atomic force microscopy (AFM), and quartz crystal microbalance with dissipation monitoring (QCM-D). The data are compared with small-angle X-ray scattering (SAXS) results obtained with lipid vesicle/peptide solutions. The peptide membrane interaction is shown to be significantly concentration dependent. At low concentrations, the peptide inserts at the outer leaflet in the interface between the headgroup and tail core. Insertion of the peptide results in a slight decrease in the lipid packing order of the bilayer, although not sufficient to cause membrane thinning. By increasing the indolicidin concentration well above the physiologically relevant conditions, a deeper penetration of the peptide into the bilayer and subsequent lipid removal take place, resulting in a slight membrane thinning. The results suggest that indolicidin induces lipid removal and that mixed indolicidin-lipid patches form on top of the supported lipid bilayers. Based on the work presented using model membranes, indolicidin seems to act through the interfacial activity model rather than through the formation of stable pores.

1. Introduction

Antimicrobial peptides (AMPs) show promising potential as future antibiotics with potent activity against a broad spectrum of pathogens. AMPs are part of the innate immune response found in all classes of life, including humans, animals, fungi, and bacteria. A wide range of AMPs extracted from different species found in nature have so far been studied for their potential as future antibiotics. The mode of action of antimicrobial peptides has extensively researched creating a consensus that membrane binding and membrane destabilization is a key function in the AMPs ability to kill bacteria [1–4]. Overcoming non-specific membrane destabilization would require a more profound redesign of the bacteria which is difficult to achieve through mutation and therefore AMPs have a significantly lower risk of developing resistance. Despite a great number of scientific studies, the precise molecular mechanism for the membrane interaction is not yet fully unveiled. This is mainly due to the experimental challenges in detecting the peptide insertion and associated small structural alterations within the membrane, in particular at physiologically relevant concentrations.

Scattering and imaging techniques, as small-angle X-ray/neutron scattering (SAXS/SANS) for solutions [5–24], neutron reflectometry (NR) for surfaces [25–32] and atomic force microscopy (AFM) [33,34] have been extensively used to study the structure of model lipid membranes. Moreover, the internal structure of living bacteria (including the cytoplasmic membrane) has been resolved using a combination of small and wide angle X-ray scattering [35]. With these methods, the interaction between peptides and model membrane can be investigated with high resolution in situ at low peptide concentrations. Lipid bilayers are often used as models of cellular membranes either in the form of free floating bilayers in solution or as supported lipid bilayers (SLBs) on solid surfaces. SLBs in combination with a set of surface sensitive techniques enable morphological, overall binding and detailed structural investigation of peptide interaction with model cellular membranes [32,36]. On the other hand, free floating lipid bilayers such as unilamellar lipid vesicles (ULVs) give complementary insight into the interaction between model membranes and AMPs that lack the unavoidable influence of the supporting substrate [5,6,23,24,37,38]. Despite its simplicity, the scattering signal from the bulk solution approach gives the orientational average structures. This complex system thus demands significant effort in theoretical modelling in real space to

* Corresponding author.
E-mail address: reidar.lund@kjemi.uio.no (R. Lund).

https://doi.org/10.1016/j.bbamem.2019.04.003
Received 8 February 2019; Received in revised form 22 March 2019; Accepted 7 April 2019
Available online 09 April 2019

extract detailed structural data from the experimental results. Here, we combine bulk scattering and surface scattering techniques to overcome the limitations of these techniques and exploit their complementarities.

Ideally to fully mimic the cell membrane of bacteria the lipid composition of the model membranes should include the natural lipids found in bacteria membranes, for example a lipid extract with mainly phosphatidylethanolamine (PE), phosphatidylglycerol (PG) lipids and cardiolipin in the case of the gram-negative bacteria *Escherichia coli*. However, simpler membrane mimics including pure lipids with known molecular volumes and chemical structure are necessary in order to extract detailed structural information from the scattering data. Conventionally, either pure phosphatidylcholine (PC) lipids or a combination of PC and PG lipids have been used as a substitute in formation of supported lipid bilayers as model membrane systems [25,27,29,33,39–44]. Recently, it was shown that stable SLBs can be formed with a combination of PE and PC lipids [45], although a preparation of model supported bilayers with both PE and negative charged PG lipids is to the authors' knowledge yet to be reported in literature. Therefore, in this study we use PC-PG lipids as a simple model bacterial membrane.

Most conventional AMPs are α-helical peptides, and these have been vastly studied using various scattering techniques and model membranes resulting in the proposal of several possible molecular modes of actions. The literature is quite extensive in this respect so we will briefly describe a few examples: Maculatin 1.1 (21 residues, net charge +3) was found to cause a slight thickening of the membrane and the peptide translocated through passive diffusion as measured by neutron reflectometry [46]. The shorter aurein 1.2 (13 residues, net charge +2), on the other hand, led to a slight degree of membrane thinning with the peptide being integrated into the lipid tail region rather than translocating across the membrane [25]. This led to the conclusion that aurein 1.2 acts via the carpet model. In the carpet model, the peptide initially binds to the lipid surface and covers the membrane as a carpet, which over time and upon increased peptide surface concentration results in disintegration of the membrane in a detergent like manner [1,25]. A study using grazing incidence diffraction (GID) on multilamellar lipid membranes on solid supports, demonstrates that magainin 2 (23 residues, net charge +5) adsorb to the bilayer at low peptide-lipid ratio, while translocation of the peptide occurred at higher amounts of peptide [39,47]. The peptide was also found to promote significant disordering in the lamellar stacking of the lipids in the membrane [42]. However interestingly, no experimental evidence for pore formation was found in this study [39] contrary to what has been reported in the past using neutron off-specular scattering [48]. A similar concentration dependency was also seen for alamethicin (20 residues, net charge −1) [49], which perturbs the membrane by causing non-lamellar lipid structures as observed by X-ray diffraction [50]. A combination of diffuse X-ray scattering at small and wide angles in stacked multilayered membrane samples and NR of single lipid bilayers showed that the cyclic peptide colistin (11 residues, net charge +5) partitions deeper towards the hydrocarbon middle region of membranes mimicking the outer membrane of Gram negative bacteria [7]. As seen from the literature the proposed mechanism of AMPs does not only vary according to the conformational shape of the peptides, but can also be linked to the size of the peptide. Comparing synthetic peptides with varying size has indicated that smaller peptides are able to penetrate into the bilayer affecting the lipid phase and ordering [25,29], while larger sized peptides situated on the surface of the membrane [27]. The effect of peptide size, conformational shape and hydrophobicity needs to be further studied to get a better understanding of the impact on the mechanism of action.

Here, we systematically study the structural interaction between AMP, indolicidin (13 residues, net charge +4) extracted from bovine neutrophils, and model lipid membranes made of PC and PG lipids. Contrary to the peptides used in the studies mentioned above, indolicidin has been found to be largely unstructured in solution [6,51,52] and retains a Gaussian chain structure with ~1% fibers as seen by SAXS [6]. Earlier studies suggest that addition of indolicidin results in local membrane thinning and solubilisation as determined by AFM [34], while partial insertion into the bilayer and removal of lipids at higher concentrations (≥5 μM) was suggested by quartz crystal microbalance with dissipation monitoring (QCM-D) [40]. However a recent SAXS study revealed that at physiologically relevant low peptide to lipid ratios, no significant perturbation of the lipid bilayer was detected [6]. In this work we will investigate these interactions in more detail using a multitude of experimental techniques with different structural resolution using the same model lipid membrane. This is achieved by comparing high resolution neutron and X-ray scattering techniques; NR and SAXS with AFM and QCM-D. Apart from comparing the methods and investigating the structural interactions of flat versus curved bilayers, this allows us to gain detailed insights into the lipid interaction of indolicidin. Indolicidin was chosen for this study because of its simple structure and small size enabling us to more straightforwardly model and deduce its interaction with membranes. Furthermore, indolicidin is one of the most studied natural AMPs. However, its lipid interaction has not previously been studied using neutron reflectometry. The data reveal that the peptide perturbs the lipid membrane without any clear pore formation as previously suggested [51], without causing significant thinning of the bilayers as observed for other small peptides [29,53].

2. Experimental section

2.1. Materials and sample preparation

Synthetic DMPC (1,2-dimyristoyl-sn-glycero-3-phosphocholine), DMPG (1,2-dimyristoyl-sn-glycero-3-phospho-(1′-rac-glycerol)), and DMPE-PEG(1,2-dimyristoyl-sn-glycero-3-phosphoethanolamine-N-[methoxy(polyethylene glycol)-2000]) were purchased from Avanti Polar Lipids and used as received without further purification. Lipid stocks were prepared in volume ratios of 1:3 methanol:chloroform and mixed in the correct proportions to give the same mass as the aimed final vesicle solution.

The SLBs for the NR, QCM-D and AFM experiments were created through fusion of tip sonicated vesicles as previously described [54]. In short, the lipid were dissolved in chloroform/methanol and mixed according to the desired molar ratio. The solvent was then removed under a stream of nitrogen, and the vials left in vacuum for at least 1 h. Lipid films were then kept at −20 °C until use. Immediately prior to the experiments, the lipid films were hydrated with MilliQ water to a concentration of 0.2 mg/ml and incubated for 1 h at 35 °C. The solution was then sonicated using a tip sonicator for 10 min on a 50% duty cycle (5 s on/off). The solution was mixed 1:1 with a 4 mM $CaCl_2$ solution immediately prior to formation of lipid bilayers. The lipid suspension in $CaCl_2$ was injected into the cell and left for approximately 10 min to equilibrate prior to extensive rinsing with buffer. In all the experiments, both the clean surface and the pristine lipid bilayer were fully characterized prior to peptide injection.

For preparation of 100 nm unilamellar liposomes for SAXS experiments, 2.5 mol% of DMPE-PEG was added in addition to DMPC and DMPG to sterically stabilize the liposomes against phase separation upon peptide addition. In the preparation, the organic solvent was removed completely under vacuum using a Heidolph rotary evaporator with a Vacuubrand vacuum pump. The resulting lipid film was hydrated with 50 mM tris(hydroxymethyl) aminomethane buffer (tris-buffer), pH 7.4, for at least 1 h at ~10 °C above the melting temperature of the lipid mixture (35 °C). After sonication for 10 min, the lipid dispersions were extruded through a 100 nm pore diameter polycarbonate filter (> 21 times) using an Avanti mini-extruder fitted with two 1 ml airtight syringes.

Indolicidin (ILPWKWPWWPWRR-$CONH_2$) was synthesized using standard 9-fluorenylmethyloxycarbonyl protecting group (Fmoc)

chemistry with 2-(1H-benzotriazol-1-yl)-1,1,3,3-tetramethyluronium hexafluorophosphate (HBTU) and *N*-Methylmorpholine (NMM) as coupling reagents on an automated peptide synthesizer (ResPep SL; Intavis Bioanalytical Instruments AG) in a 15 μmol scale in micro-columns using a 4-Methylbenzhydrylamine hydrochloride (MBHA) resin (0.65 mmol/g). After completion of the peptide chain, the peptide were cleaved from the resin using TFA:H_2O:TIS (95:2.5:2.5) for 2 × 1 h. Crude peptide was purified by preparative reverse-phase HPLC system consisting of Waters™ 600 Pump, In-line Degasser, 600 Controller and 2996 Photodiode Array Detector, the column used was a Waters™ XSelect® Peptide CSH C18 OBD™, 5 μm, 19 × 250 mm on an acetonitrile-water gradient. The peptide purity was determined by analytical reverse-phase High-performance liquid chromatography (HPLC) system consisting of Waters™ 717 plus Autosampler, In-line Degasser AF, 600 Controller and 2996 Photodiode Array Detector, the column used was a Waters™ Symmetry™ C18, 5 μm, 4.6 × 250 mm on an acetonitrile-water gradient. The peptide mass was determined using a Bruker Microflex™ (MALDI-TOF-Mass Spectrometry) (see Supplementary material).

2.2. Quartz crystal microbalance with dissipation monitoring

QCM-D experiments were performed using a Q-SENSE E4 system (Qsense, Biolin Scientific, Stockholm, Sweden) with 50 nm Qsense Silicon Oxide sensors. The fundamental frequency and six overtones (3rd, 5th, 7th, 9th, 11th and 13th) were recorded during the experiment. The instrument was set to equilibrate at 37 °C before performing any measurements. The lipids were prepared using the method described above in MilliQ water and injected using a peristaltic pump (Ismatec IPC-N 4) at a flow rate of 100 μL/min. After following the SLB formation (upon reaching a frequency of −24 Hz and dissipation close to 0), the remaining lipids in the cells were rinsed off with MilliQ. Upon stabilization of the baseline, the solvent was exchanged to tris-buffer and again left to stabilize under flow. The peptide was injected in the desired concentration dissolved in tris-buffer. The experiments were performed in duplicates to validate the results.

2.3. Neutron reflectometry

Neutron reflection (NR) measurements were performed using flow-through cells and 80 × 50 × 15 mm Silica crystals from SIL'TRONIX Silicon Technologies. The reflectometer FIGARO [55] at Institut Laue-Langevin (Grenoble, France) was used to record the time-of-flight reflectivity at two angles of incidence (0.8 and 3.2°) to cover the Q-range ($Q = 4\pi \sin(\theta/2)/\lambda$ where θ is the scattering angle and λ is the neutron wavelength). The instrumental resolution was set to $\frac{\Delta\lambda}{\lambda} = 7\%$. Flow through solid-liquid cells were provided by the neutron facility. They were composed by a plastic water reservoir in close contact with the polished surface of the silicon substrates. The water reservoir was equipped with inlet and outlet connections to exchange the aqueous solution. Substrate and reservoir were sandwiched between two aluminium plates connected to a water bath for temperature regulation. The temperature, measured by a thermocouple in close contact with the silicon substrate, was maintained at 37 °C. Prior to the experiment, the crystals were fully characterized in D_2O and H_2O to determine the structural parameters of the silicon oxide layer present on the surface. After injection, the lipids were equilibrated in the cell for ~20 min before rinsing with tris-buffer, and the bilayers were characterized in three contrasts (D-tris, H-tris and 50:50H/D-tris hereafter referred to as CM3). Then, 10 ml of the peptide solution (in D-tris, CM3 and H-tris sequentially) in the desired concentration were injected into the cell at a flow rate of ~2 ml/min using a syringe pump, and the resulting system was fully characterized in all three contrasts. Finally, the membranes were measured again after rinsing with H-tris and D-tris. The use of different contrast conditions is known as the contrast variation method and it allows for simultaneous fitting of multiple reflectivity data sets, leading to an unambiguous solution and a more precise structural determination [56].

All NR profiles were analysed using an optical matrix method where the surface is modelled as sequential layers representing the substrate and lipid bilayer (three layers: one for the lipid tail and two for the hydrated head groups) as well as peptide and solvent which were allowed to penetrate the different layers freely. The fit analysis was done using the Motofit package taking into account the experimental resolution [57]. The NR data analysis provides information on the internal structure of thin films at an interface [58]. In particular, for SLBs, it allows to determine thickness, composition and surface coverage not only of the entire bilayer but of the different regions composing it, such as headgroups and hydrophobic tails. For this reason, the lipid bilayer before and after interaction with 0.8 μM indolicidin and rinsing were fitted using a 5 layer model (distinguishing silicon oxide – water – head– tail – head), while the 10 μM indolicidin bilayer after rinsing was fitted using an 8 layer model in which the 3 extra layers account for indolicidin/lipids patches forming on top of the bilayer (as single or double layers). During the fitting analysis, a model dividing the tail region into two layers to simulate asymmetric bilayers was considered. As discussed in the Supplementary material, this did not improve the quality of the fit significantly and therefore a symmetric model for the bilayer composition was chosen.

The error of the fit parameters for the thickness and solvent amount was determined by the Monte Carlo error analysis fitting algorithm included in the Motofit package [57] and reflects the quality of the fit. The area per molecule is calculated based on the fit parameters as

$$A_{mol} = \frac{V}{\varphi \cdot t}$$

where V is the volume of the lipid head/tail group (see table S1), φ is the lipid volume fraction (1-solvent [%]) and t is the thickness of the layer. The error in the area per molecule, δA_{mol}, was calculated as

$$\delta A_{mol} = \sqrt{\left(\frac{\delta\varphi}{\varphi}\right)^2 + \left(\frac{\delta t}{t}\right)^2} \cdot A_{mol}$$

2.4. Atomic force microscopy

Measurements were carried out on a Nanoscope IV multimode AFM (Veeco Instruments Inc.). Images were generated in the PeakForce Quantitative Mechanical Property Mapping® (QNM) mode with a silicon oxide tip (Olympus micro cantilever OTR8 PS-W) having a spring constant of 0.15 N/m and a radius of curvature of < 20 nm. Peak Force Tapping™ mode is different from contact and traditional tapping mode since it allows for precisely controlling the imaging force in order to keep indentations small, thus enabling non-destructive and high-resolution imaging. This mode is ideal for imaging of soft matter in liquid environments at high resolution. A liquid flow cell (glass probe holder, MTFML, Bruker Corporation) was used to scan the surfaces in a liquid environment and to exchange solution in situ. The setup was optimized for real-time continuous flow imaging where the solution constantly exchanges via a slow gravity feed [33].

First, a freshly cleaved mica surface was imaged in ultrapure water in order to ensure a clean and smooth surface (RMS: < 500 pm) prior to bilayer measurements. Small unilamellar vesicles were introduced into the AFM liquid flow cell and vesicle attachment and bilayer formation were imaged. The lipids were incubated in the AFM for at least 30 min and imaged to secure high coverage before rinsing the membrane with water. Before introducing the peptide, the membranes were rinsed in excess tris-buffer. The peptide solution was introduced to the membrane and the flow was maintained while imaging for at least 90 min. In this way, new peptides were continuously brought to the interface during scanning. Then, the membrane was rinsed with tris-buffer while imaging. All images were recorded at a resolution of 256 × 256 pixels

with a scan rate of 1 Hz. The z-setpoint and differential gains were manually optimized during each scan. Images were analysed and processed in the Gwyddion 2.22 software. The experiment was performed in duplicates to validate the results.

2.5. Small angle X-ray scattering

SAXS experiments of mixtures of peptide and liposomes were performed at the automated BM29 bioSAXS beamline [59] at the European Synchrotron Radiation Facility (ESRF) in Grenoble, France. The data was obtained using an energy of 12.5 keV and a detector distance of 2.87 m, covering a Q range of 0.0047 $Å^{-1}$ to 0.5 $Å^{-1}$. The data set was calibrated to an absolute intensity scale using water as a primary standard. 45 µL samples were run through a capillary using the flow mode of the automated sample changer [60]. SAXS data was collected in ten successive frames of 0.5 s each to monitor radiation damage and the data reduction was done using the standard tool at BM29 [61]. The SAXS results were analysed using the theoretical model described in detail in Ref. [6]. In short, the model provides a detailed description of the membrane by dividing into probability functions for each component (lipid sub-units/peptide) across the bilayer.

3. Results and discussion

3.1. Concentration dependent interaction between indolicidin and SLB

QCM-D constitutes a useful technique to screen different experimental conditions for biomolecular interaction with model membranes. The simultaneous measurement of both changes in frequency and dissipation allows us to extract information on the viscoelastic properties of the membrane due to the direct relationship between the frequency and the mass adsorbed to the surface, while the dissipation is dependent on the rigidity of the layer. For example, the typical QCM-D signal observed from an adsorption process of a rigid film is a decrease in frequency due to the addition of mass on the surface without any significant changes in the dissipation due to the rigidity. For a soft and heterogeneous film (containing water), however, an increase in the dissipation will follow the adsorption due to the dampening of the oscillations of the QCM-D sensor. Upon desorption of material from the surface, for example removal of lipids due to solubilisation, the frequency increases as a result of mass removal, while the changes in dissipation depend on the hydration and rigidity of the remaining material.

Fig. 1A–C shows the QCM-D signals upon increasing concentrations of indolicidin (1, 5 and 10 µM) added to an SLB made of DMPC-DMPG. Immediately after peptide injection, there was a significant decrease in the frequency and an increase in the dissipation for all the samples, indicating peptide adsorption to the membrane. However, the point at which the QCM-D signals reached steady state was concentration dependent. At 1 µM, the dissipation reached an inflection point and then flattened at values higher than for the original SLB. For 5 µM, on the other hand, both frequency and dissipation reached an inflection point that was followed by a slow increase in the frequency. For the highest concentration of 10 µM, the frequency and dissipation displayed different steps where a peak in frequency (and the dissipation) was followed by equilibration at values slightly higher in frequency (and lower in dissipation) than before peptide addition. These signals are typical indicators of significant lipid removal from the membrane.

Plots of Δd versus Δf with the 7th harmonic were constructed and shown in Fig. 1D to better visualise the different d/f regimes related to various steps in the indolicidin interaction with the lipid membrane. For the lower concentrations of 1 µM and 2 µM, two regimes were observed: in regime 1) there was a large increase in the dissipation that was accompanied by a large decrease in the frequency, and in regime 2) there was a region where the dissipation decreased without any significant change in the frequency that stabilized around −8 to −10 Hz. The former indicates penetration of the peptide into the bilayer while the latter signal indicates the formation of a stiffer absorbed layer. For 2 µM, the slope of the first regime was less steep than in the case of 1 µM, with a smaller increase in the dissipation over the same decrease in frequency. This behaviour might indicate a deeper insertion into the bilayer at the higher concentration, while at lower peptide concentrations the peptide occupies a more superficial location on the membrane which is reflected in an apparent less rigid structure. Similar behaviour was seen for PAMAM dendrimers at higher concentrations (up to 8 µM) [27].

For the higher indolicidin concentrations (5 and 10 µM) close to the reported minimum inhibitory concentration (MIC) value of indolicidin (8–16 µM dependent on the type of bacteria) [62], the slope for regime 1 was similar to the one observed for the lower concentrations (Fig. 1D), although the rate of the initial binding was significantly higher than the lower concentrations (Fig. 1A–C). The initial rapid binding at higher concentrations agreed with reported data for zwitterionic PC membranes and indolicidin [40]. However, regime 2 differed from the one observed for the lower concentrations giving an increase in frequency which was accompanied by a small dissipation. The inflection points between regime 1 and 2 occurred at −6 Hz and −8 Hz for 5 and 10 µM, respectively. Finally, for 10 µM indolicidin steady state was achieved at a higher frequency than the original bilayer. Regime 2 for the highest peptide concentrations indicated a loss of wet mass at the surface, pointing towards peptide-induced solubilisation of the phospholipid membrane. Similar results were previously obtained for higher indolicidin concentrations on pure PC membranes [40]. The difference in the behaviour of the dissipation between 5 and 10 µM might be a result of the peptide penetrating deeper into the bilayer resulting in more rigid membranes. Aurein 1.2, that resembles indolicidin in size, was shown to cause similar behaviour by QCM-D where addition of high concentrations (20 µM) resulted in a steady state frequency higher than the initial baseline [25].

Although the QCM-D measurements point towards different steps in the molecular mechanism of action between indolicidin and lipid membranes as a function of peptide concentration, they could not provide any structural information on the changes induced in the lipid membrane. Therefore, experiments were carried out using NR on the same system to provide higher resolution information of the structural interaction of the AMP. Fig. 2A, B and C show the reflectivity profiles, best fits and SLD profiles for DMPC/DMPG (90/10) bilayers before and after exposure to either 0.8 (1:10 peptide-lipid ratio) or 10 µM (~1:1 peptide lipid ratio) indolicidin in two solvent contrasts (H_2O and D_2O). The structural parameters for the pristine SLBs were similar and thus only one of the SLB reflectivity curves are shown in Fig. 2 (Table 1 gives the parameters used to fit the data). The full data sets for the two SLBs are given in the Supplementary material Fig. S2.

From the fit analysis of the pristine SLBs NR data, we obtained a thickness and area per lipid that was comparable with literature values based on MD simulations and SAXS data on DMPC/DMPG phospholipids [9,13,63]. Moreover, the SLDs obtained were in agreement with the theoretical SLD values for the lipid mixture as shown in Table S1. Moreover, the total bilayer thickness seemed unaffected by exposure to 0.8 µM peptide, while a slight decrease from 38 to 36 Å was seen for the bilayers exposed to 10 µM indolicidin. This slight thinning is, however, within the error of the fit analysis. Furthermore, peptide addition caused a change in the fitted SLD values for both lipid headgroup and core as compared to that for pure lipid bilayers. For 10 µM indolicidin, peptide addition resulted in changes of the SLD profile throughout the whole bilayer, while 0.8 µM mainly affected the SLD profile for the outer headgroup and the tail region. The observed changes in SLD are explained by the peptide having a different SLD than the lipids thus resulting in a change in the average SLDs of the modelled layers upon insertion of the peptide (see Table S1).

The NR fit analysis of the 0.8 µM indolicidin data (1:10 peptide to lipid ratio) indicates that the peptide inserted into the outer headgroup

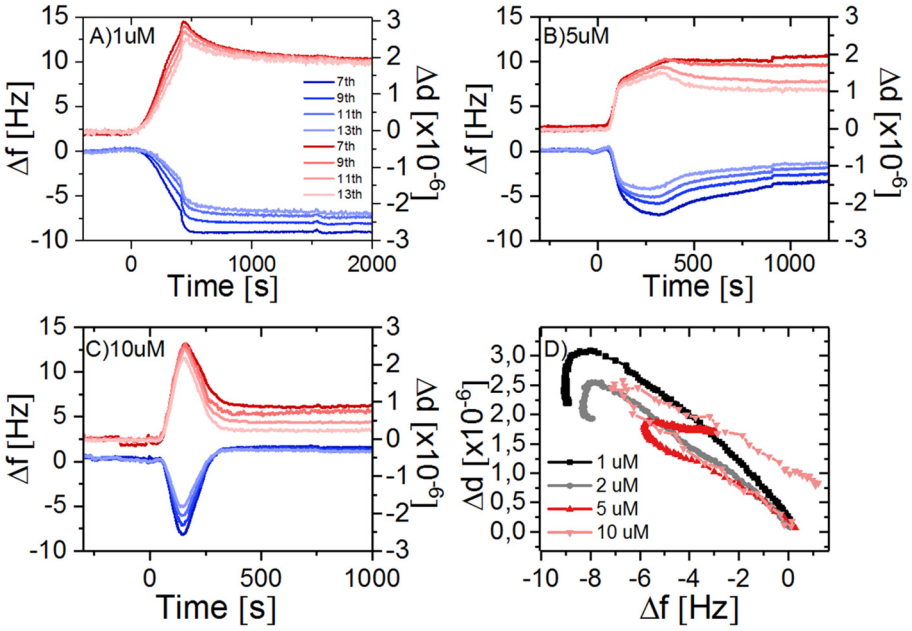

Fig. 1. QCM-D results showing addition of indolicidin to supported lipid bilayers composed of DMPC and DMPG in a molar ratio of 9:1. Three concentrations of indolicidin 1 μM (A), 5 μM (B) and 10 μM (C) were added to the bilayers at $t = 0$ s in a continuous flow. Changes in frequency are shown in blue and dissipation in red. For clarity, four overtones are plotted (see legend in panel A). Both the frequency and dissipation at all the harmonics are normalized to zero before addition of the peptide. The supported lipid bilayer formation is not shown in the plot (see the Supplementary material Fig. S1 for an example of typical SLB formation). (D) Change in dissipation against change in frequency with increasing concentration (1 μM, 2 μM, 5 μM and 10 μM). For clarity, only the 7th harmonic is shown, and the frequency and dissipation are offset to 0 before addition of the peptide. (For interpretation of the references to color in this figure legend, the reader is referred to the web version of this article.)

and tail region of the bilayer and did not affect the inner headgroup. For 10 μM (approximately 1:1 ratio) indolicidin, the peptide penetrated deeper into the bilayer which could be observed as a change in the average SLD of the inner headgroup region in Fig. 2B. The amount of peptide inserted in the head region of the membrane could readily be calculated from the SLD values and it increased significantly from 0 to 60% in the inner head group and 13 to 36% in the outer headgroup when increasing the concentration of the peptide from 0.8 to 10 μM. On the other hand, the amount of peptide incorporated in the tail region did not seem to be affected by the peptide concentration and remained at 17%. This points towards a clear affinity of the peptide for the head-tail interface also upon penetration to the inner leaflet.

3.2. Lipid removal caused by peptide insertion

Table 1 shows that the bilayer coverage decreased significantly for 10 μM indolicidin, implying that more lipids were removed from the membrane as the peptide (surface) concentration increased. Lipid removal is in agreement with our QCM-D experiments (Fig. 1), where injection of 10 μM indolicidin led to a decrease in mass on the sensor explained as removal of phospholipids from the bilayer. The changes in the thickness and solvent fraction of the tail region indicated that the peptide significantly disturbed the ordering of the tails, which is also corroborated by DSC experiments published in a recent work by Nielsen et al. [6].

In Fig. 3, the NR and SLD profile of the bilayer exposed to 0.8 μM is shown before and after extensive rinsing with tris-buffer using three contrasts (D-tris, H-tris and cm3-tris). Note that this is different from Fig. 2 where we only compare the samples in the presence of peptide and prior to rinsing with buffer. The corresponding fit parameters for the SLB in the presence of indolicidin and extensive rinse are shown in Table 1, while those fit parameters for the data of 0.8 μM showing the bilayer before rinsing is given in Table S1 in the Supplementary material. The inset in Fig. 3 shows the reduced reflectivity, RQ^4, plotted against Q to highlight the appearance of a distinct peak at the Q range of 0.10–0.13 $Å^{-1}$ upon incubation with indolicidin (marked with an arrow in Fig. 3A). This peak was clear for the H-tris data due to the high contrast towards the deuterated lipids. This contribution was modelled by addition of two mixed lipid/peptide layers (it was seen that two extra layers were needed to fully explain the data), separated by a thin water layer (6 Å). The coverage of the middle lipid/peptide layer (in direct contact with the SLB) was 27% for 0.8 μM, while the outer lipid/

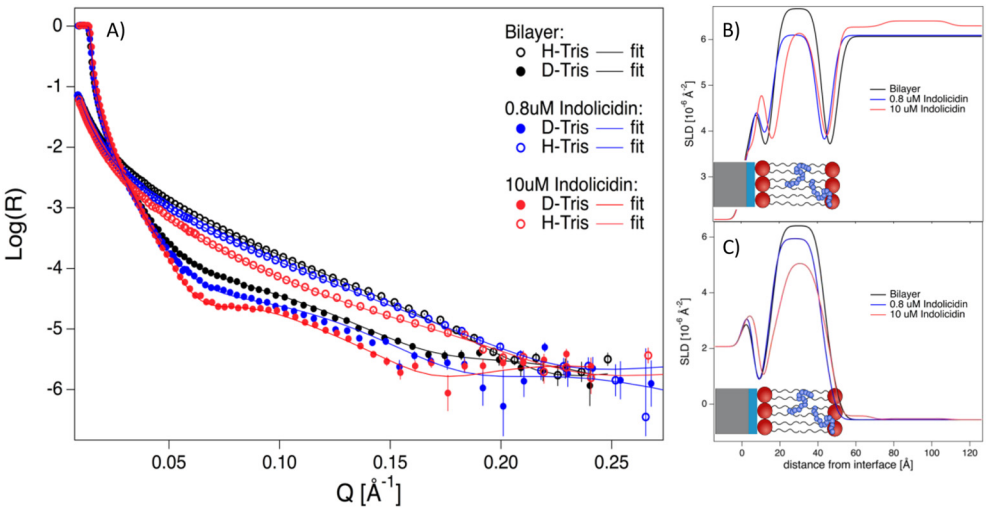

Fig. 2. NR measurements of DMPC-DMPG SLBs before and after addition of 0.8 and 10 μM indolicidin. (A) Reflectivity profiles together with the best fits (lines) to the described models. SLD profiles obtained from the fit analysis against distance from the interface for an SLB before and after being exposed to indolicidin in the indicated concentration of D-contrast (B) and H-contrast (C). In this case, 10 ml of the peptide was flushed into the cell and rinsed off with buffer prior to the NR measurements (the experiments with the two concentrations were performed in separate cells). The slight difference in the SLD of the bulk is due to incomplete exchange of the solution when changing contrast (and typically accounts by for example 3% H2O presence in the D2O contrast).

Table 1
Fitted parameters for tail-deuterated DMPC/DMPG membranes prior to and after exposure to 0.8 μM and 10 μM indolicidin and extensive rinse with buffer. A_{mol} is the molecular area per lipid component including solvent. The amount of indolicidin incorporated in the different layers is estimated based on the change in SLD observed after exposure to the peptide. As seen from the table, increasing the concentration of indolicidin from 0.8 to 10 μM results in deeper penetration of the peptide into the bilayer causing higher lipid removal.

Layer	d [Å]	Solvent [%]	SLD [10^{-6} Å^{-2}]	Indolicidin %	d [Å]	Solvent [%]	SLD [10^{-6} Å^{-2}]	Indolicidin %
Pristine SLB								
Water	3	100	–	–	4 ± 1	100	–	–
Head (inner)	6 ± 1	18 ± 3	1.83	–	6 ± 1	13 ± 3	1.83	–
Tail	25 ± 1	4 ± 1	6.7	–	26 ± 1	1 ± 1	6.7	–
Head (upper)	6 ± 1	18 ± 3	1.83	–	6 ± 1	13 ± 3	1.83	–
Total thickness (Å)	37 ± 2		A_{mol} 64 ± 2 Å^2		38 ± 2		A_{mol} 60 ± 1 Å^2	
SLB after addition of			0.8 μM indolicidin				10 μM indolicidin	
Water	3	100	–	–	4 ± 1	100	–	–
Head (inner)	6 ± 1	19 ± 3	1.83	–	8 ± 1	13 ± 3	2.6	60 ± 3
Tail/indolicidin	25 ± 1	6 ± 1	6.1	17 ± 1	21 ± 1	15 ± 2	6.1	17 ± 1
Head/indolicidin	6 ± 1	10 ± 4	2	13 ± 2	7 ± 1	13 ± 3	2.3	36 ± 2
Total thickness (Å)	37 ± 2		A_{mol} N/A		36 ± 2		A_{mol} N/A	
Indolicidin/lipid	–	–	–	–	27 ± 5	98 ± 1	5.2 ± 0.4	10 ±
Water	–	–	–	–	6 ± 1	100	–	
Indolicidin/lipid	–	–	–	–	34 ± 1	98 ± 1	6.0 ± 0.4	0

peptide layer had a low coverage of only 2%. The SLD for both of these layers were found to be 5.6 10^{-6} Å^2 indicating that these patches mainly are composed of phospholipids, with only around 4% peptide.

Rinsing with buffer induced major changes in the reflectivity profile with disappearance of the peak at intermediate Q. Therefore, these patches seem to be relatively loosely attached structures. The thickness of the patches was similar to the thickness of one bilayer i.e. 37 Å. These patches might originate from peptide/lipids complexes (for example mixed micelles) as suggested from the SLD values obtained from the analysis. Their low surface coverage is compatible with the amount of lipids removed from the bilayer by the insertion of the peptide (17%). Indeed, we observed a change in the composition of the lipid core layer allowing to include the inserted peptide as described above. This mechanism is illustrated in Scheme 1. Lipid removal can be explained by the decrease in the energy barrier against solubilisation of individual lipids in the outer leaflet of the bilayer upon peptide integration in the bilayer. This is a typical behaviour for the interaction of biosurfactants with lipid membranes including surfactin, which is a natural lipopeptide surfactant with antibiotic properties. In this case, progressive lipid removal takes place upon reaching a threshold biosurfactant concentration [43]. The removal of lipids due to peptide insertion is characteristic for the detergent-like interaction mechanism that has been reported for a series of linear amphipathic cationic peptides resulting in gradual membrane disintegration [64].

No evidence of distinct pores or channels in the membrane was observed at 0.8 μM indolicidin, a concentration that can be considered as physiologically relevant. Under this condition, the peptide did not seem to affect the inner headgroup and the bilayer coverage remained stable even as lipids were exchanged by peptides. These results on simple model membranes might suggest that the mechanism of indolicidin is linked to disordering of the lipids in the bilayer upon peptide insertion rather than defined pore formation. A possible explanation of why pore-formation could not be seen in the case of indolicidin may be linked to the lack of a secondary structure in solution. Both melittin [44] and magainin [48] are examples of peptides with an alpha-helical secondary structure that have shown to form pores by quasi elastic neutron scattering (QENS) together with AFM and off-specular neutron reflectometry. The alpha-helical secondary structure may be essential for the clustering of the peptides in the membrane resulting in the formation of barrel-stave or toroidal pores. Peptide induced lipid disordering, as we observe for indolicidin, was suggested by Wimley, among others, to cause lysis of bacteria and eventually, cell death [2].

The formation of lipid/peptide patches upon addition of indolicidin could visually be followed by time resolved AFM imaging, and analysis of the corresponding height profiles (Fig. 4). In Fig. 4A and B, the preformed SLB is shown as evidenced by the presence of a few defects of ~4 nm in depth, which is in agreement with the fit parameters from NR on the same type of SLBs as shown in Table 1 and typical for a DMPC/DMPG bilayer [9,13,63]. The bilayer defects disappeared immediately after a continuous flow of 0.8 μM indolicidin solution was flushed over the bilayer, and new patches were formed on top of the bilayer (seen as light dots in Fig. 4C). This suggests that indolicidin readily integrated and filled the defects present in the SLB. From the height profile in Fig. 4D, the height of these patches could be determined to be 3.5–4 nm and 7–8 nm and thus correspond to a single or double peptide-lipid bilayer in perfect agreement with the results from the fit analysis of the NR data. The formation of these patches happened on the time scale of

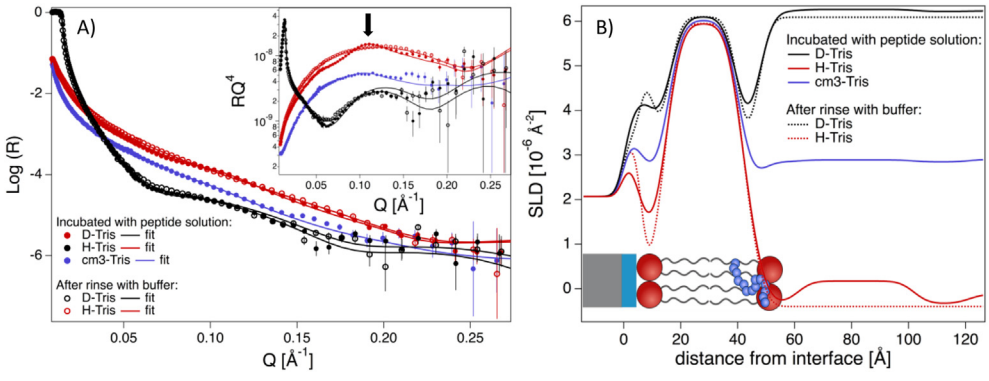

Fig. 3. NR measurements of a DMPC-DMPG SLB after being exposed to 0.8 μM indolicidin and after rinsing with buffer. A) Reflectivity profiles for the measurements together with the best fit. Inset shows the same curves plotted in a RQ^4 against Q to increase the visibility of the change in high Q after rinsing. B) SLD profiles resulting from the fit analysis against distance from the interface for an SLB before and after rinsing with buffer. Inset illustrates the proposed position of the peptide in the membrane resulting from the fit. The arrow marks the peak that arises from the repetition of peptide/lipid patches on top of the SLB.

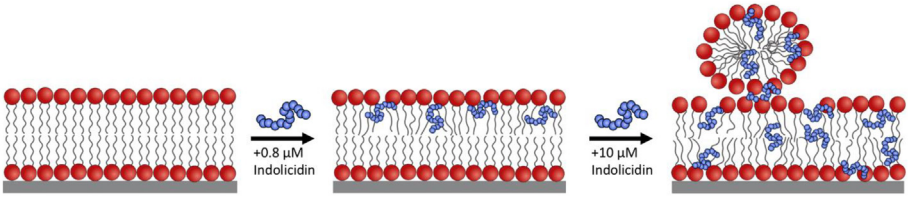

Scheme 1. Illustration of concentration dependent interaction of indolicidin with lipid bilayers based on fit analysis of SAXS and NR results.

minutes in the AFM experiment and did not change appearance with incubation with the peptide over a time period of approximately 2 h. When the membrane was subsequently rinsed with tris-buffer, however, most of the mixed lipid/peptide structures were removed as seen in Fig. 4E and F, also in agreement with our NR results. In contrast to the NR experiment, not all the single bilayer patches were removed as seen from the AFM image and the corresponding height profile. An explanation to this discrepancy could be that the flow rate in the AFM experiment was significantly lower than for NR. A very low flow rate (~50 μL/min) in AFM is necessary in order to enable imaging under flow. This might lead to less efficient removal of the lipid/peptide patches.

3.3. Comparing reflectivity results for supported lipid bilayers with SAXS data of unilamellar lipid vesicles

In order to compare the SLB results with unilamellar lipid vesicles, we performed SAXS experiments on peptide-vesicle samples with similar lipid: peptide ratios. The SAXS results for DMPC-DMPG-DMPE-PEG liposomes with and without added indolicidin (1:10) are shown in Fig. 5A. DMPE-PEG was added in the vesicle formulation to prevent aggregation of vesicles upon peptide addition, but that should not affect the interaction with peptides due to the low molar ratio of 2.5%. The data was fitted using the asymmetric scattering density profile model (SDP), as developed by Nagle, Kučerka and co-workers [8,10,11,15] modified to account for the peptide scattering as described by Nielsen et al. [6]. Fit analysis of the scattering curves for the liposomes gave a membrane thickness of 37.4 Å and an area per lipid of 60 Å^2, in agreement with the results found in the NR data analysis (Table 1). In Fig. 5, the SLD profiles calculated from the fit parameters from both SAXS and NR are shown for comparison. The curves representing the peptide-free membrane (red) found from the two methods virtually overlap except for the oscillation in neutron SLD at the inner leaflet for NR representing the silicon surface below the bilayer. The latter is not relevant in the case of SAXS where free floating unilamellar vesicles (ULVs) are used.

Upon addition of indolicidin, a shift in the X-ray scattering curve at intermediate Q took place as shown in Fig. 5A. For SAXS data of lipid bilayers the minimum in the scattering curve at intermediate Q is highly sensitive to the negative contrast, i.e. lower electron density than water of the lipid tails and positive contrast (higher electron density) of the headgroups. Through theoretical modelling, it was found that this shift in the minima upon peptide addition was caused by a change in the scattering contrast as the peptide inserted into the bilayer. The insertion is clearly visible due to the peptide having a higher electron density than the lipids (as seen in Table S1 of the Supplementary material). The SAXS data analysis suggests that the peptide inserted at the interface between the head and tail region on the outer leaflet of the membrane as a random coil. This is illustrated in the volume probability curve showing the membrane structure with the additional Gaussian peak representing the peptide inserting in the membrane (Fig. 5B).

To facilitate the comparison between the SAXS and NR results, the electron density profile from our SAXS measurements was converted to a neutron SLD profile in H_2O and plotted together with the SLD profile obtained from NR analysis (for 0.8 μM as the lipid: peptide ratio in these two cases were similar) and plotted in Fig. 5C. Both NR and SAXS data did not show major changes in the bilayer structure, as the overall

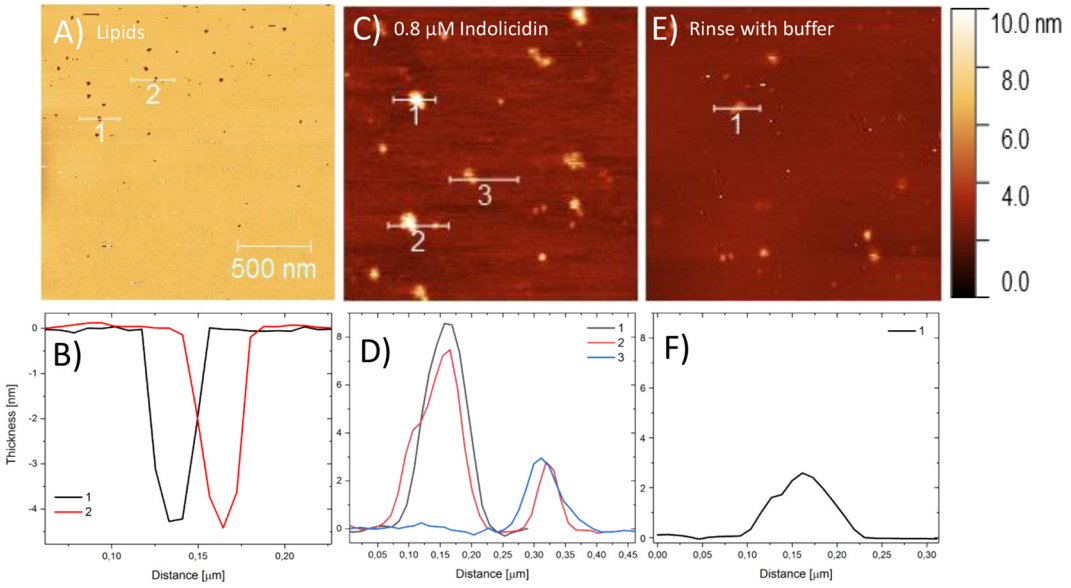

Fig. 4. Time-lapse series of AFM images of a lipid bilayer made of DMPC and DMPG captured under continuous flow of the indicated solution. The scale bar in A applies to all images. A) SLB formed on a Mica surface with good coverage but some remaining holes allowing for measurements of the thickness of the bilayer from the height profile of two indicated pores as seen in B). C) 0.8 μM indolicidin flowed over the surface resulting in disappearance of the visible holes in the bilayer and formation of bilayer patches with height profiles shown in graph D). E) SLB after rinsing with buffer resulting in removal of most of the patches and a decrease in the height of the patches shown in graph F.

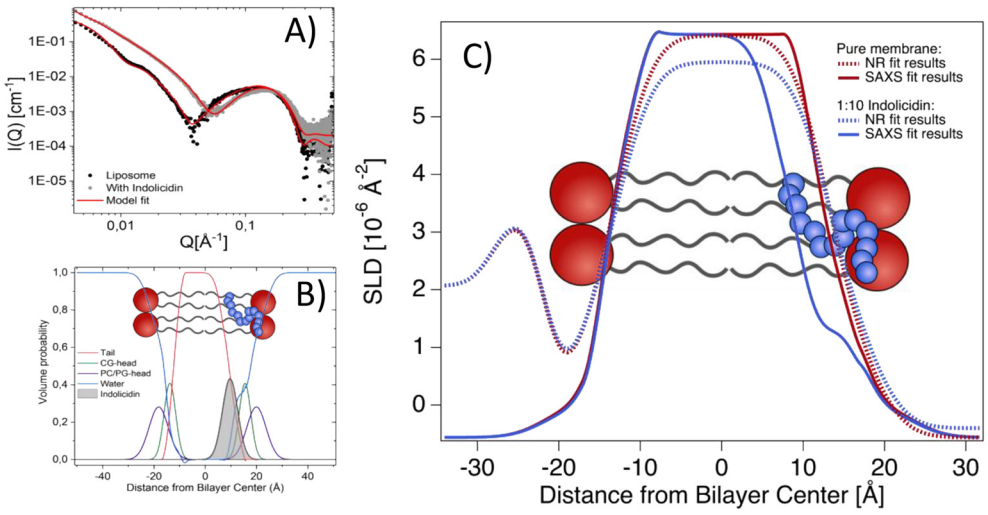

Fig. 5. Comparison with previously reported small angle X-ray scattering results for liposomes exposed to indolicidin [6]. A) Scattering curves and model fits for liposomes with and without peptide. B) Illustration of the volume probability distribution for the bilayer with the peptide positioned in the interface between the headgroups and the tail region on the outer leaflet of the membrane. C) Comparison of the neutron SLD profile derived from the NR experiment (- - -) and SAXS experiment (—) (the latter is converted from X-ray to neutron SLD to directly compare the two methods). The distance z = 0 marks the centre of the bilayer.

thickness of the bilayer remained constant. However, in SAXS experiments, peptide to lipid ratios above 1:10 showed a ~3 Å thinning of the bilayer [6], which is also supported by molecular dynamics simulations for this peptide [53,65].

The model used to analyse the NR data is the traditional slab model that does not allow to extract the exact position of the peptide. Instead each layer is averaged with a common SLD. Further division of the lipid core layer into two layers to model peptide asymmetry did not lead to an improved fit quality but rather over-parametrization. This might be due to the lack of contrast, in particular between the peptide and lipid head (see the SLD values given in Table S1). Therefore, we used the symmetric profile to analyse the data to prevent over-interpretation of the data and to minimise the number of fitting parameters. However, a fit to a model allowing for an asymmetric peptide position in the bilayer (see details of the model in Fig. S3) is included in the Supplementary material to show that the NR data does not contradict the SAXS modelling of an asymmetric distribution (Fig. S4).

In Fig. 5C, a comparison of the peptide effect on the bilayer as seen for both NR and SAXS is presented by the corresponding SLD profiles for the 1:10 peptide-lipid samples. The SLD profile from the NR results showed a decreased plateau of the SLD in the middle of the bilayer representing the tail region when compared to the pure bilayer. This is due to the peptide having a lower SLD than the deuterated tail. The effect that the peptide insertion had on the outer headgroups of the lipid bilayer was not easily detected using NR, as mentioned above. For SAXS, the sensitivity to changes in electron density as the peptide incorporates in the bilayer allowed us to determine the specific peptide location [6]. When comparing the SLD profile from NR with the one from SAXS we could see that the effect indolicidin had on the SLD profile was localised in the outer leaflet (interface between head and tail). The deeper penetration of the peptide seen from the NR SLD profile, might be due to lack of sensitivity of the method as described above. However, the deeper penetration might also additionally be explained by the use of SLBs formed on negatively charged silicon oxide surfaces that could attract the positively charged peptide deeper into the bilayer. Although the NR fit allowed only up to 4 ± 1 vol% solvent in the tail region prior to peptide interaction, small pre-existing defects (holes) in the SLB (as seen visually by AFM in Fig. 4) could facilitate deeper peptide penetration into the membrane. However, as indolicidin has some polar sidechains, as well as hydrophobic aromatic groups, it is likely from a physical chemical perspective that the peptide will insert in the interface between the head group that is partly hydrated and the lipid tail region. It is less likely that indolicidin will position only in the non-hydrated tail region.

4. Conclusion

The combination of NR, QCM-D, AFM and SAXS allowed us to establish the structural interaction of indolicidin, a naturally occurring antimicrobial peptide, with a model lipid bilayer. Our data suggest that the insertion of indolicidin in the bilayer is strongly dependent on the concentration. From QCM-D and NR, we conclude that indolicidin interacts mainly with the outer headgroup and tail region at lower concentrations (≤ 2 μM) while the peptide penetrates deeper into the bilayer diffusing also into the inner headgroup at higher concentrations (≥ 5 μM). Interestingly, the resulting effect on the bilayer thickness is also concentration dependent. Low concentrations of indolicidin cause no changes to the thickness or overall structure of the bilayer, while higher concentrations result in a disordering of the bilayer and a slight thinning of the bilayer. Similar trends were observed for lipid vesicles probed by SAXS. Combination of the information of the peptide insertion from these methods provides good evidence in support of the "interfacial activity" scenario presented by Wimley [2] where the peptide causes a disordering of the lipids in the bilayer by inserting in the interface between the lipid head and tail region. This is believed to result in lysis of bacteria and eventual cell death, however, further studies using lipid compositions closer mimicking bacteria membrane needs to be studied to fully elucidate the mode of action. Further, indolicidin seems to dissolve lipids in the membrane resulting in the formation of lipid/peptide patches on the supported lipid bilayer as seen by AFM and NR and in an increase in the size of the vesicles as seen by SAXS.

In this work we show how detailed analysis of scattering techniques on supported lipid bilayers as well as unilamellar lipid vesicles, together with QCM-D and AFM imaging, are high resolution biophysical techniques for the study of peptide interactions with model lipid membranes.

Transparency document

The Transparency document associated with this article can be found, in online version.

Acknowledgements

JEN, AL, PRH, MC, HJ and RL gratefully acknowledge NordForsk (Project no. 82004), and JEN, MC and RL acknowledge InterReg MAX4ESSFUN (project no. UiO-006) for financial support. The authors are also grateful to the ILL for providing beamtime (https://doi.org/10.5291/ILL-DATA.9-13-743) and for the assistance by Armando Maestro and Sarah Waldie at ILL during the NR experiments at Figaro. We are

also grateful to the ESRF for SAXS beamtime at BM29, and the PSCM lab for support during both the NR and SAXS experiment. We acknowledge use of the Norwegian national infrastructure for X-ray diffraction and scattering (RECX). We would also like to thank Victoria Ariel Bjørnestad for her contribution to the SAXS experiments and the modelling of SAXS data.

Appendix A. Supplementary data

Supplementary data to this article can be found online at https://doi.org/10.1016/j.dummy.2019.01.002.

References

[1] L.T. Nguyen, E.F. Haney, H.J. Vogel, The expanding scope of antimicrobial peptide structures and their modes of action, Trends Biotechnol. 29 (2011) 464–472, https://doi.org/10.1016/j.tibtech.2011.05.001.
[2] W.C. Wimley, Describing the mechanism of antimicrobial peptide action with the interfacial activity model, ACS Chem. Biol. 5 (2010) 905–917, https://doi.org/10.1021/cb1001558.
[3] R.E. Hancock, A. Rozek, Role of membranes in the activities of antimicrobial cationic peptides, FEMS Microbiol. Lett. 206 (2002) 143–149, https://doi.org/10.1111/j.1574-6968.2002.tb11000.x.
[4] H. Jenssen, P. Hamill, R.E. Hancock, Peptide antimicrobial agents, Clin. Microbiol. Rev. 19 (2006) 491–511, https://doi.org/10.1128/CMR.00056-05.
[5] T. Narayanan, D. Weerakkody, A.G. Karabadzhak, M. Anderson, O.A. Andreev, Y.K. Reshetnyak, pHLIP peptide interaction with a membrane monitored by SAXS, J. Phys. Chem. B 120 (2016) 11484–11491, https://doi.org/10.1021/acs.jpcb.6b06643.
[6] J.E. Nielsen, V.A. Bjørnestad, R. Lund, Resolving the structural interactions between antimicrobial peptides and lipid membranes using small-angle scattering methods: the case of indolicidin, Soft Matter 14 (2018) 8750–8763, https://doi.org/10.1039/C8SM01888J.
[7] F.G. Dupuy, I. Pagano, K. Andenoro, M.F. Peralta, Y. Elhady, F. Heinrich, S. Tristram-Nagle, Selective interaction of colistin with lipid model membranes, Biophys. J. 114 (2018) 919–928, https://doi.org/10.1016/j.bpj.2017.12.027.
[8] J.B. Klauda, N. Kučerka, B.R. Brooks, R.W. Pastor, J.F. Nagle, Simulation-based methods for interpreting X-ray data from lipid bilayers, Biophys. J. 90 (2006) 2796–2807, https://doi.org/10.1529/biophysj.105.075697.
[9] N. Kučerka, Y. Liu, N. Chu, H.I. Petrache, S. Tristram-Nagle, J.F. Nagle, Structure of fully hydrated fluid phase DMPC and DLPC lipid bilayers using X-ray scattering from oriented multilamellar arrays and from unilamellar vesicles, Biophys. J. 88 (2005) 2626–2637, https://doi.org/10.1529/biophysj.104.056606.
[10] N. Kučerka, J.F. Nagle, J.N. Sachs, S.E. Feller, J. Pencer, A. Jackson, J. Katsaras, Lipid bilayer structure determined by the simultaneous analysis of neutron and X-ray scattering data, Biophys. J. 95 (2008) 2356–2367, https://doi.org/10.1529/biophysj.108.132662.
[11] N. Kucerka, J. Pencer, J.N. Sachs, J.F. Nagle, J. Katsaras, Curvature effect on the structure of phospholipid bilayers, Langmuir 23 (2007) 1292–1299, https://doi.org/10.1021/la062455t.
[12] J. Nagle, M. Wiener, Relations for lipid bilayers. Connection of electron density profiles to other structural quantities, Biophys. J. 55 (1989) 309–313, https://doi.org/10.1016/S0006-3495(89)82806-1.
[13] J. Pan, F.A. Heberle, S. Tristram-Nagle, M. Szymanski, M. Koepfinger, J. Katsaras, N. Kučerka, Molecular structures of fluid phase phosphatidylglycerol bilayers as determined by small angle neutron and X-ray scattering, Biochim. Biophys. Acta Biomembr. 1818 (2012) 2135–2148, https://doi.org/10.1016/j.bbamem.2012.05.007.
[14] J. Pan, D.P. Tieleman, J.F. Nagle, N. Kučerka, S. Tristram-Nagle, Alamethicin in lipid bilayers: combined use of X-ray scattering and MD simulations, Biochim. Biophys. Acta Biomembr. 1788 (2009) 1387–1397, https://doi.org/10.1016/j.bbamem.2009.02.013.
[15] B. Eicher, F.A. Heberle, D. Marquardt, G.N. Rechberger, J. Katsaras, G. Pabst, Joint small-angle X-ray and neutron scattering data analysis of asymmetric lipid vesicles, J. Appl. Crystallogr. 50 (2017), https://doi.org/10.1107/S1600576717000656.
[16] F.A. Heberle, J. Pan, R.F. Standaert, P. Drazba, N. Kučerka, J. Katsaras, Model-based approaches for the determination of lipid bilayer structure from small-angle neutron and X-ray scattering data, Eur. Biophys. J. 41 (2012) 875–890, https://doi.org/10.1007/s00249-012-0817-5.
[17] F.A. Heberle, R.S. Petruzielo, J. Pan, P. Drazba, N. Kučerka, R.F. Standaert, G.W. Feigenson, J. Katsaras, Bilayer thickness mismatch controls domain size in model membranes, J. Am. Chem. Soc. 135 (2013) 6853–6859, https://doi.org/10.1021/ja3113615.
[18] J.D. Nickels, S. Chatterjee, C.B. Stanley, S. Qian, X. Cheng, D.A. Myles, R.F. Standaert, J.G. Elkins, J. Katsaras, The in vivo structure of biological membranes and evidence for lipid domains, PLoS Biol. 15 (2017) e2002214, , https://doi.org/10.1371/journal.pbio.2002214.
[19] D.K. Rai, S. Qian, Interaction of the antimicrobial peptide aurein 1.2 and charged lipid bilayer, Sci. Rep. 7 (2017) 3719, , https://doi.org/10.1038/s41598-017-03795-6.
[20] S. Qian, W.T. Heller, Peptide-induced asymmetric distribution of charged lipids in a vesicle bilayer revealed by small-angle neutron scattering, J. Phys. Chem. B 115 (2011) 9831–9837, https://doi.org/10.1021/jp204045t.
[21] C.-C. Lee, Y. Sun, S. Qian, H.W. Huang, Transmembrane pores formed by human antimicrobial peptide LL-37, Biophys. J. 100 (2011) 1688–1696, https://doi.org/10.1016/j.bpj.2011.02.018.
[22] S. Qian, W. Wang, L. Yang, H.W. Huang, Structure of the alamethicin pore reconstructed by X-ray diffraction analysis, Biophys. J. 94 (2008) 3512–3522, https://doi.org/10.1529/biophysj.107.126474.
[23] V. Castelletto, R.H. Barnes, K.-A. Karatzas, C.J. Edwards-Gayle, F. Greco, I.W. Hamley, R. Rambo, J. Seitsonen, J. Ruokolainen, Arginine-containing surfactant-like peptides: interaction with lipid membranes and antimicrobial activity, Biomacromolecules (2018), https://doi.org/10.1021/acs.biomac.8b00391.
[24] V. Castelletto, R.H. Barnes, K.-A. Karatzas, C.J. Edwards-Gayle, F. Greco, I.W. Hamley, J. Seitsonen, J. Ruokolainen, Restructuring of lipid membranes by an arginine-capped peptide bolaamphiphile, Langmuir (2018), https://doi.org/10.1021/acs.langmuir.8b01014.
[25] D.I. Fernandez, A.P. Le Brun, T.C. Whitwell, M.-A. Sani, M. James, F. Separovic, The antimicrobial peptide aurein 1.2 disrupts model membranes via the carpet mechanism, Phys. Chem. Chem. Phys. 14 (2012) 15739–15751, https://doi.org/10.1039/C2CP43099A.
[26] A. Åkesson, T. Lind, N. Ehrlich, D. Stamou, H. Wacklin, M. Cárdenas, Composition and structure of mixed phospholipid supported bilayers formed by POPC and DPPC, Soft Matter 8 (2012) 5658–5665, https://doi.org/10.1039/C2SM00013J.
[27] A. Åkesson, T.K. Lind, R. Barker, A. Hughes, M. Cárdenas, Unraveling dendrimer translocation across cell membrane mimics, Langmuir 28 (2012) 13025–13033, https://doi.org/10.1021/la3027144.
[28] T.K. Lind, Understanding peptide dendrimer interactions with model cell membrane mimics, in, Department of Chemistry, Faculty of Science, University of Copenhagen, 2014.
[29] T.K. Lind, L. Darre, C. Domene, Z. Urbanczyk-Lipkowska, M. Cárdenas, H. Wacklin, Antimicrobial peptide dendrimer interacts with phosphocholine membranes in a fluidity dependent manner: a neutron reflection study combined with molecular dynamics simulations, Biochim. Biophys. Acta, Biomembr. 1848 (2015) 2075–2084, https://doi.org/10.1016/j.bbamem.2015.05.015.
[30] Y. Gerelli, L. Porcar, G. Fragneto, Lipid rearrangement in DSPC/DMPC bilayers: a neutron reflectometry study, Langmuir 28 (2012) 15922–15928, https://doi.org/10.1021/la303662e.
[31] Y. Gerelli, L. Porcar, L. Lombardi, G. Fragneto, Lipid exchange and flip-flop in solid supported bilayers, Langmuir 29 (2013) 12762–12769, https://doi.org/10.1021/la402708u.
[32] A. Martel, L. Antony, Y. Gerelli, L. Porcar, A. Fluitt, K. Hoffmann, I. Kiesel, M. Vivaudou, G. Fragneto, J.J. De Pablo, Membrane permeation versus amyloidogenicity: a multitechnique study of islet amyloid polypeptide interaction with model membranes, J. Am. Chem. Soc. 139 (2016) 137–148, https://doi.org/10.1021/jacs.6b06985.
[33] T.K. Lind, P. Zielinska, H.P. Wacklin, Z. Urbanczyk-Lipkowska, M. Cárdenas, Continuous flow atomic force microscopy imaging reveals fluidity and time-dependent interactions of antimicrobial dendrimer with model lipid membranes, ACS Nano 8 (2013) 396–408, https://doi.org/10.1021/nn404530z.
[34] J.E. Shaw, J.-R. Alattia, J.E. Verity, G.G. Privé, C.M. Yip, Mechanisms of antimicrobial peptide action: studies of indolicidin assembly at model membrane interfaces by in situ atomic force microscopy, J. Struct. Biol. 154 (2006) 42–58, https://doi.org/10.1016/j.jsb.2005.11.016.
[35] E.F. Semeraro, J.M. Devos, L. Porcar, V.T. Forsyth, T. Narayanan, In vivo analysis of the Escherichia coli ultrastructure by small-angle scattering, IUCrJ 4 (2017) 751–757, https://doi.org/10.1107/S2052252517013008.
[36] S. Bobone, Y. Gerelli, M. De Zotti, G. Bocchinfuso, A. Farrotti, B. Orioni, F. Sebastiani, E. Latter, J. Penfold, R. Senesi, Membrane thickness and the mechanism of action of the short peptaibol trichogin GA IV, Biochim. Biophys. Acta Biomembr. 1828 (2013) 1013–1024, https://doi.org/10.1016/j.bbamem.2012.11.033.
[37] G. Pabst, S.L. Grage, S. Danner-Pongratz, W. Jing, A.S. Ulrich, A. Watts, K. Lohner, A. Hickel, Membrane thickening by the antimicrobial peptide PGLa, Biophys. J. 95 (2008) 5779–5788, https://doi.org/10.1529/biophysj.108.141630.
[38] E. Sevcsik, G. Pabst, W. Richter, S. Danner, H. Amenitsch, K. Lohner, Interaction of LL-37 with model membrane systems of different complexity: influence of the lipid matrix, Biophys. J. 94 (2008) 4688–4699, https://doi.org/10.1529/biophysj.107.123620.
[39] C. Münster, A. Spaar, B. Bechinger, T. Salditt, Magainin 2 in phospholipid bilayers: peptide orientation and lipid chain ordering studied by x-ray diffraction, Biochim. Biophys. Acta Biomembr. 1562 (2002) 37–44, https://doi.org/10.1016/S0005-2736(02)00357-7.
[40] K.F. Wang, R. Nagarajan, T.A. Camesano, Differentiating antimicrobial peptides interacting with lipid bilayer: molecular signatures derived from quartz crystal microbalance with dissipation monitoring, Biophys. Chem. 196 (2015) 53–67, https://doi.org/10.1016/j.bpc.2014.09.003.
[41] K. Hristova, W.C. Wimley, V.K. Mishra, G. Anantharamiah, J.P. Segrest, S.H. White, An amphipathic α-helix at a membrane interface: a structural study using a novel X-ray diffraction method, J. Mol. Biol. 290 (1999) 99–117, https://doi.org/10.1006/jmbi.1999.2840.
[42] C. Münster, J. Lu, B. Bechinger, T. Salditt, Grazing incidence X-ray diffraction of highly aligned phospholipid membranes containing the antimicrobial peptide magainin 2, Eur. Biophys. J. 28 (2000) 683–688, https://doi.org/10.1007/s002490050008.
[43] H.-H. Shen, R.K. Thomas, J. Penfold, G. Fragneto, Destruction and solubilization of supported phospholipid bilayers on silica by the biosurfactant surfactin, Langmuir

26 (2010) 7334–7342, https://doi.org/10.1021/la904212x.
[44] Z. Buck, J. Torres, A. Miskowiec, E. Mamontov, H. Kaiser, F. Hansen, H. Taub, M. Tyagi, L. Collins, K. Herwig, Effect of melittin on water diffusion and membrane structure in DMPC lipid bilayers, EPL 123 (2018) 18002, , https://doi.org/10.1209/0295-5075/123/18002.
[45] A.M. Sendecki, M.F. Poyton, A.J. Baxter, T. Yang, P.S. Cremer, Supported lipid bilayers with phosphatidylethanolamine as the major component, Langmuir 33 (2017) 13423–13429, https://doi.org/10.1021/acs.langmuir.7b02323.
[46] D.I. Fernandez, A.P. Le Brun, T.-H. Lee, P. Bansal, M.-I. Aguilar, M. James, F. Separovic, Structural effects of the antimicrobial peptide maculatin 1.1 on supported lipid bilayers, Eur. Biophys. J. 42 (2013) 47–59, https://doi.org/10.1007/s00249-012-0796-6.
[47] T. Salditt, Lipid–peptide interaction in oriented bilayers probed by interface-sensitive scattering methods, Curr. Opin. Struct. Biol. 13 (2003) 467–478, https://doi.org/10.1016/S0959-440X(03)00113-1.
[48] S.J. Ludtke, K. He, W.T. Heller, T.A. Harroun, L. Yang, H.W. Huang, Membrane pores induced by magainin, Biochemistry 35 (1996) 13723–13728, https://doi.org/10.1021/bi9620621.
[49] H.W. Huang, Y. Wu, Lipid-alamethicin interactions influence alamethicin orientation, Biophys. J. 60 (1991) 1079–1087, https://doi.org/10.1016/S0006-3495(91)82144-0.
[50] K. Lohner, E.J. Prenner, Differential scanning calorimetry and X-ray diffraction studies of the specificity of the interaction of antimicrobial peptides with membrane-mimetic systems, Biochim. Biophys. Acta Biomembr. 1462 (1999) 141–156, https://doi.org/10.1016/S0005-2736(99)00204-7.
[51] T.J. Falla, D.N. Karunaratne, R.E. Hancock, Mode of action of the antimicrobial peptide indolicidin, J. Biol. Chem. 271 (1996) 19298–19303, https://doi.org/10.1074/jbc.271.32.19298.
[52] A. Rozek, C.L. Friedrich, R.E. Hancock, Structure of the bovine antimicrobial peptide indolicidin bound to dodecylphosphocholine and sodium dodecyl sulfate micelles, Biochemistry 39 (2000) 15765–15774, https://doi.org/10.1021/bi000714m.
[53] C. Neale, J.C. Hsu, C.M. Yip, R. Pomes, Indolicidin binding induces thinning of a lipid bilayer, Biophys. J. 106 (2014) L29–L31, https://doi.org/10.1016/j.bpj.2014.02.031.
[54] B.W. König, S. Krueger, W. Orts, C.F. Majkrzak, N.F. Berk, J. Silverton, K. Gawrisch, Neutron reflectivity and atomic force microscopy studies of a lipid bilayer in water adsorbed to the surface of a silicon single crystal, Langmuir 12 (1996) 1343–1350, https://doi.org/10.1021/la950580r.
[55] R. Campbell, H. Wacklin, I. Sutton, R. Cubitt, G. Fragneto, FIGARO: the new horizontal neutron reflectometer at the ILL, Eur. Phys. J. Plus 126 (2011) 107, , https://doi.org/10.1140/epjp/i2011-11107-8.
[56] T. Crowley, E. Lee, E. Simister, R. Thomas, The use of contrast variation in the specular reflection of neutrons from interfaces, Phys. B Condens. Matter 173 (1991) 143–156, https://doi.org/10.1016/0921-4526(91)90044-F.
[57] A. Nelson, Co-refinement of multiple-contrast neutron/X-ray reflectivity data using MOTOFIT, J. Appl. Crystallogr. 39 (2006) 273–276, https://doi.org/10.1107/S0021889806005073.
[58] J. Penfold, R. Thomas, The application of the specular reflection of neutrons to the study of surfaces and interfaces, J. Phys. Condens. Matter 2 (1990) 1369, https://doi.org/10.1088/0953-8984/2/6/001.
[59] P. Pernot, A. Round, R. Barrett, A. De Maria Antolinos, A. Gobbo, E. Gordon, J. Huet, J. Kieffer, M. Lentini, M. Mattenet, Upgraded ESRF BM29 beamline for SAXS on macromolecules in solution, J. Synchrotron Rad. 20 (2013) 660–664, https://doi.org/10.1107/S0909049513010431.
[60] A. Round, F. Felisaz, L. Fodinger, A. Gobbo, J. Huet, C. Villard, C.E. Blanchet, P. Pernot, S. McSweeney, M. Roessle, BioSAXS sample changer: a robotic sample changer for rapid and reliable high-throughput X-ray solution scattering experiments, Acta Crystallogr. Sect. D: Biol. Crystallogr. 71 (2015) 67–75, https://doi.org/10.1107/S1399004714026959.
[61] A. De Maria Antolinos, P. Pernot, M.E. Brennich, J. Kieffer, M.W. Bowler, S. Delageniere, S. Ohlsson, S. Malbet Monaco, A. Ashton, D. Franke, ISPyB for BioSAXS, the gateway to user autonomy in solution scattering experiments, Acta Crystallogr. Sect. D: Biol. Crystallogr. 71 (2015) 76–85, https://doi.org/10.1107/S1399004714019609.
[62] H.M. Jindal, C.F. Le, M.Y. Mohd Yusof, R.D. Velayuthan, V.S. Lee, S.M. Zain, D.M. Isa, S.D. Sekaran, Antimicrobial activity of novel synthetic peptides derived from indolicidin and ranalexin against Streptococcus pneumoniae, PLoS One 10 (2015) e0128532-e0128532, , https://doi.org/10.1371/journal.pone.0128532.
[63] N. Kučerka, M.-P. Nieh, J. Katsaras, Fluid phase lipid areas and bilayer thicknesses of commonly used phosphatidylcholines as a function of temperature, Biochim. Biophys. Acta Biomembr. 1808 (2011) 2761–2771, https://doi.org/10.1016/j.bbamem.2011.07.022.
[64] B. Bechinger, K. Lohner, Detergent-like actions of linear amphipathic cationic antimicrobial peptides, Biochim. Biophys. Acta Biomembr. 1758 (2006) 1529–1539, https://doi.org/10.1016/j.bbamem.2006.07.001.
[65] J.C. Hsu, C.M. Yip, Molecular dynamics simulations of indolicidin association with model lipid bilayers, Biophys. J. 92 (2007) L100–L102, https://doi.org/10.1529/biophysj.107.108050.